Electronic Supplementary Information

An organometal halide perovskite photocathode integrated with a MoS_2 catalyst for efficient and stable photoelectrochemical water splitting

Hojoong Choi,‡[a] Sehun Seo,‡[a] Ju-Hyeon Kim,[a,b] Jong-Hoon Lee,[a,c] Seungkyu Kim,[a] Guangxia Piao,[d] Hyunwoong Park,[d] Kwanghee Lee*[a,b,e] and Sanghan Lee*[a]

[a] School of Materials Science and Engineering, Gwangju Institute of Science and Technology, Gwangju, 61005, Republic of Korea.

[b] Heeger Center for Advanced Materials, Gwangju Institute of Science and Technology, Gwangju, 61005, Republic of Korea.

[c] Department of Energy Resources, Huree University of Information and Communication Technology, Ulaanbaatar, 16061-0036, Mongolia.

[d] School of Energy Engineering, Kyungpook National University, Daegu, 41566, Republic of Korea.

[e] Research Institute for Solar and Sustainable Energies, Gwangju Institute of Science and Technology, Gwangju, 61005, Republic of Korea.

‡ These authors contributed equally to this work.

*E-mail address: klee@gist.ac.kr (K. L.); sanghan@gist.ac.kr (S. L.)

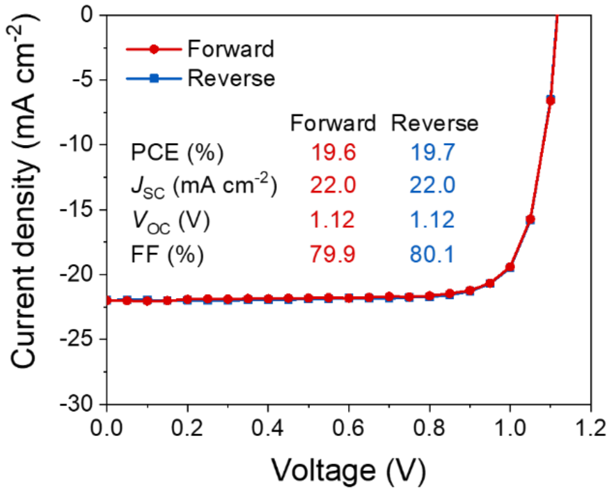

Fig. S1 Current density−voltage (J−V) curve of OHP photovoltaic (PV) cell based on methylammonium lead triiodide ($MAPbI_3$) with L-proline amino acid in the forward and reverse scan directions.

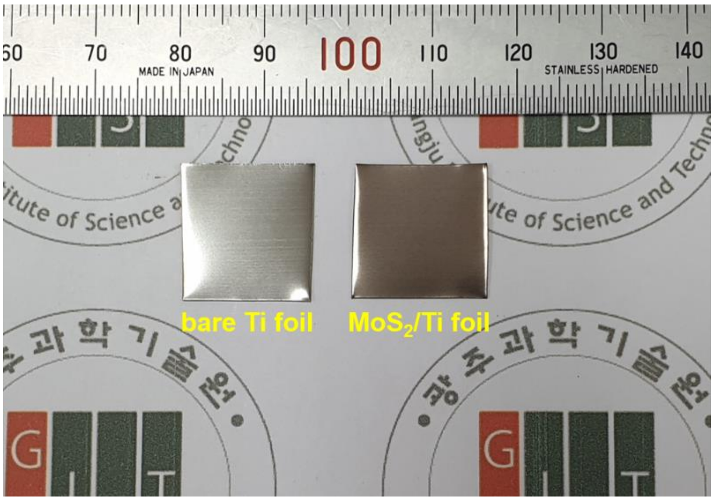

Fig. S2 Photograph of the bare Ti foil and MoS_2/Ti foil.

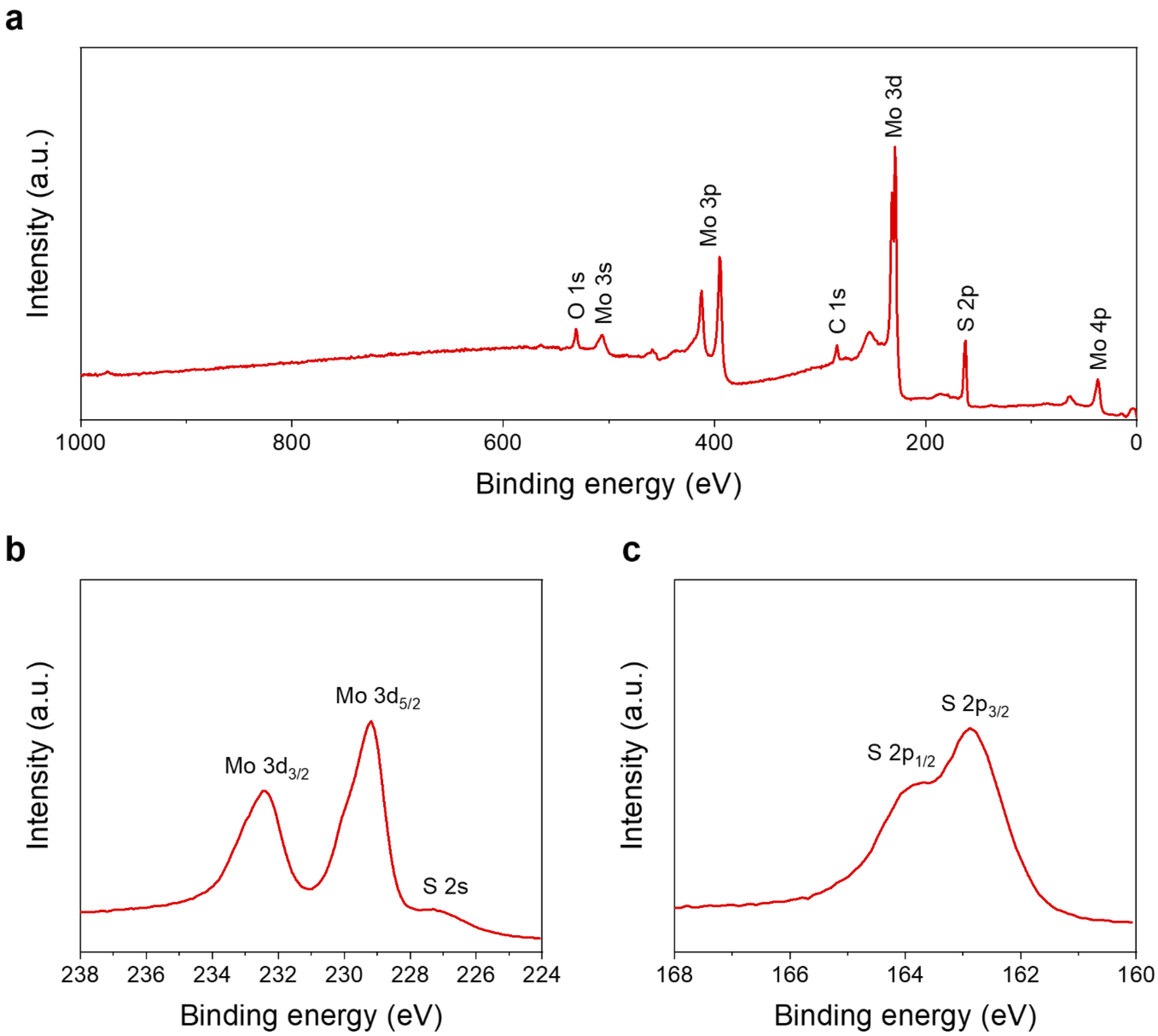

Fig. S3 X-ray photoelectron spectroscopy (XPS) spectra of MoS_2/Ti foil. (a) XPS survey spectra and high-resolution XPS spectra of (b) Mo 3d and (c) S 2p regions of MoS_2/Ti foil.

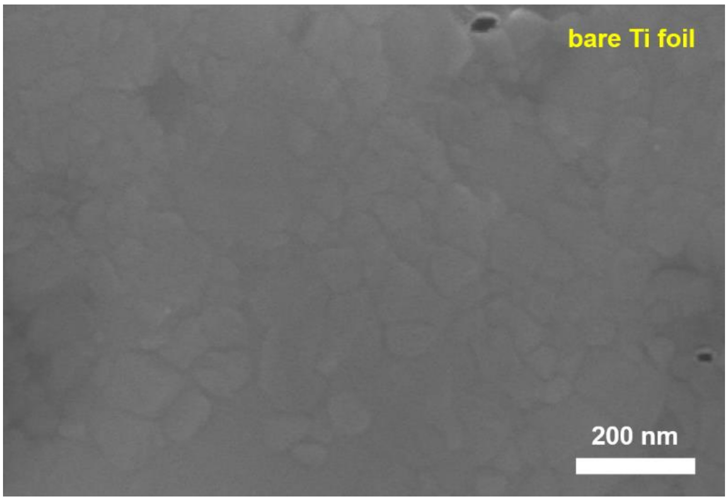

Fig. S4 Field emission scanning electron microscopy (FESEM) image of bare Ti foil.

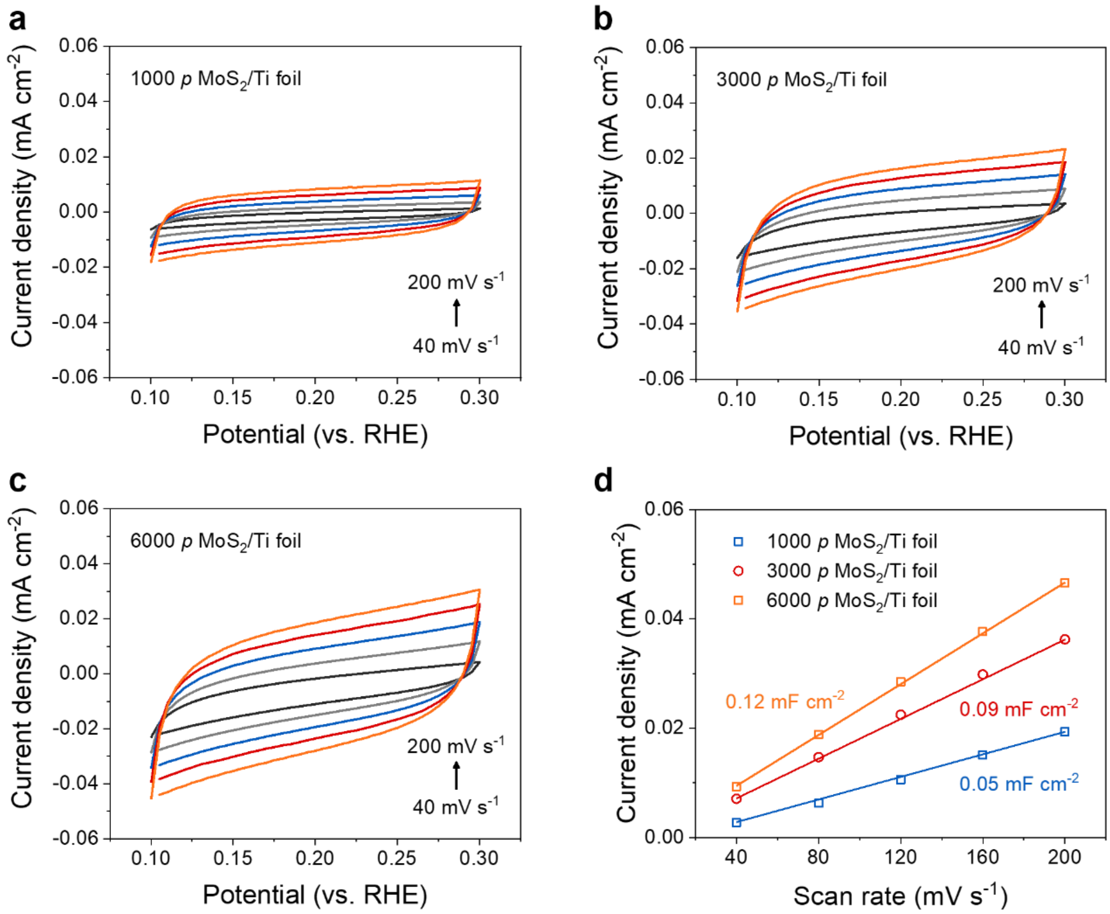

Fig. S5 Cyclic voltammetry (CV) curves of (a) 1000, (b) 3000, and (c) 6000 *p* MoS_2/Ti foils at scan rates in the range of 40−200 mV s^{-1}. (d) Estimation of double layer capacitance (C_{dl}) for 1000, 3000, and 6000 *p* MoS_2/Ti foils.

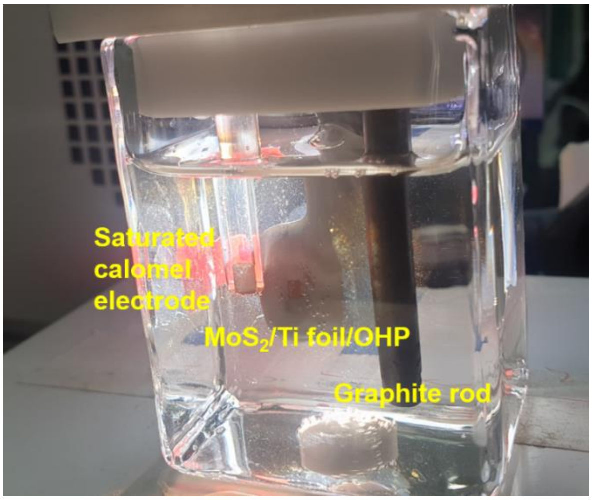

Fig. S6 Photograph of three-electrode configuration with MoS_2/Ti foil/OHP, saturated calomel electrode (SCE), and graphite rod as working, reference, and counter electrode, respectively.

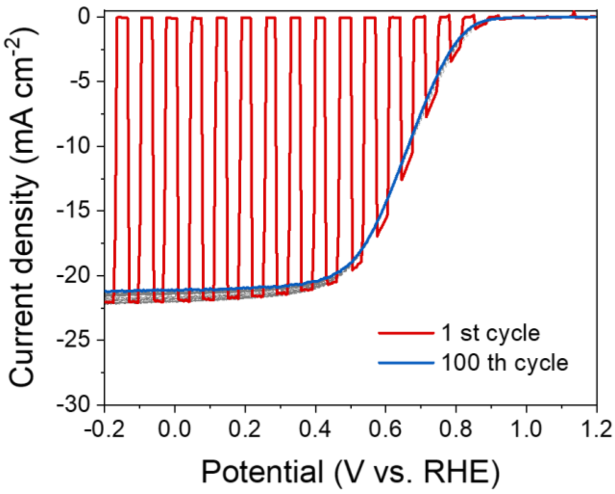

Fig. S7 Repetitive 100 cycles of LSV curves of the MoS_2/Ti foil/OHP photocathode.

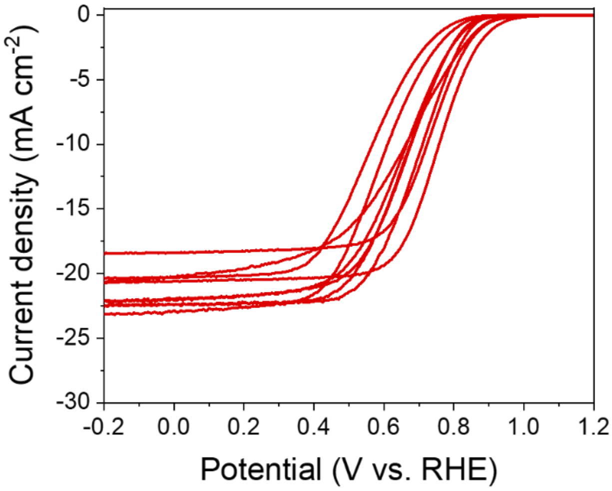

Fig. S8 LSV curves of a total 10 MoS_2/Ti foil/OHP photocathodes.

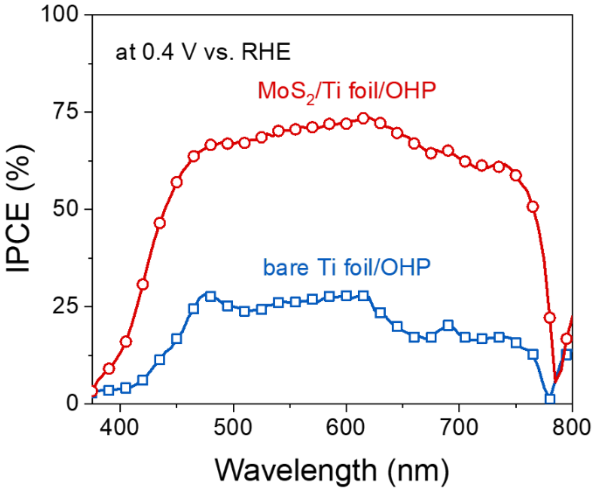

Fig. S9 Incident photon-to-electron conversion efficiency (IPCE) spectra of bare Ti foil/OHP and MoS_2/Ti foil/OHP photocathodes at a potential of a 0.4 V versus reversible hydrogen electrode (vs. RHE).

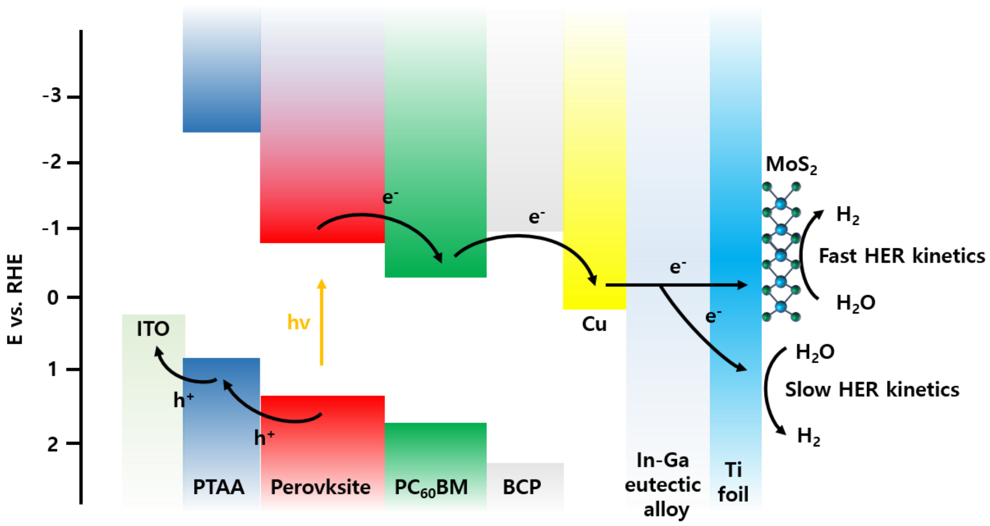

Fig. S10 Band alignment of OHP photocathodes with or without the MoS_2 HER catalyst.

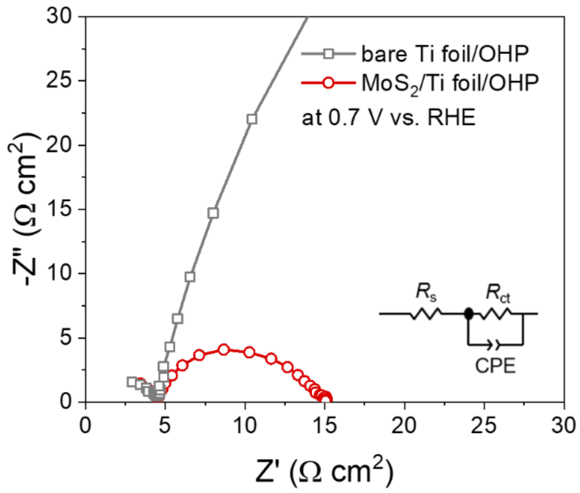

Fig. S11 Nyquist plots of bare Ti foil/OHP and MoS_2/Ti foil/OHP photocathodes measured at 0.7 V vs. RHE under illumination. The inset shows the equivalent circuit used to fit the Nyquist plots.

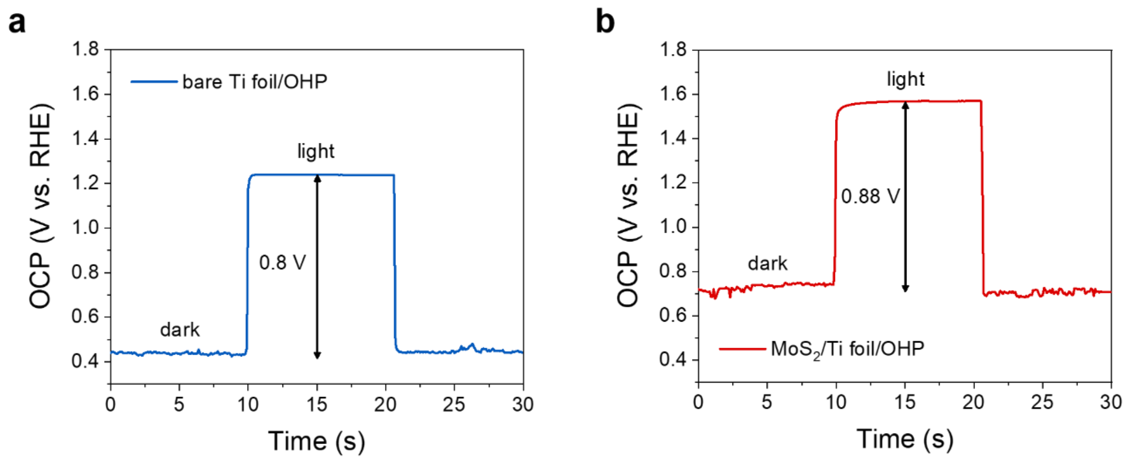

Fig. S12 Open-circuit potential (OCP) of (a) bare Ti foi/OHP and (b) MoS_2/Ti foil/OHP photocathodes in the dark and under illumination.

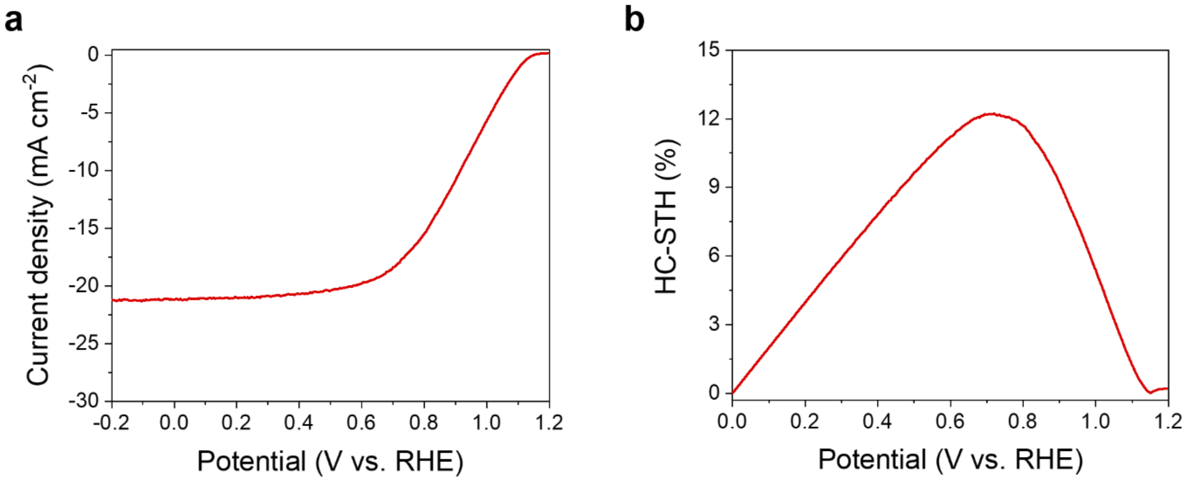

Fig. S13 (a) LSV curve and (b) corresponding half-cell solar-to-hydrogen conversion efficiency (HC-STH) of Pt/Ti foil/OHP photocathode.

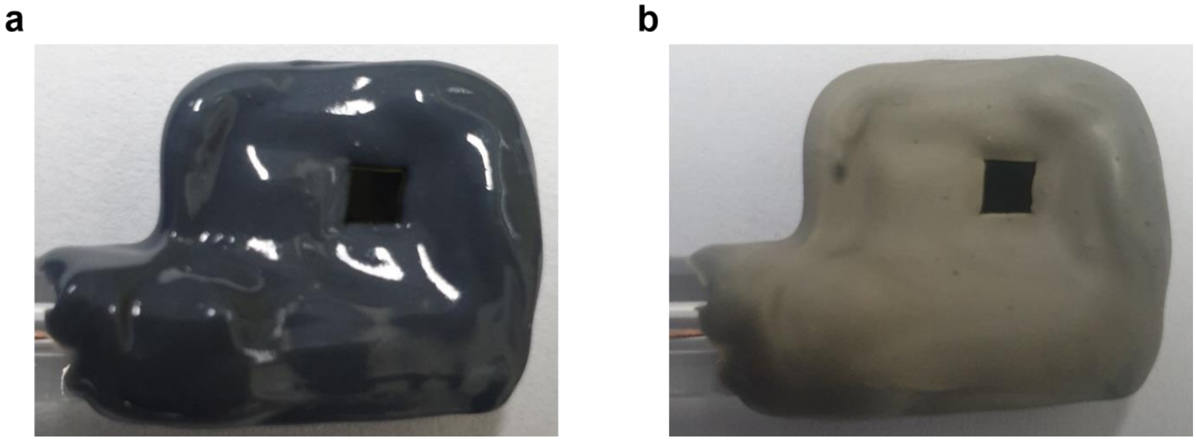

Fig. S14 Photographs of epoxy resin sealed MoS_2/Ti foil/OHP photocathode. (a) Before and (b) after the measurement of PEC stability.

Table S1 Photoelectrochemical (PEC) performance of previously reported state-of-the-art photocathodes.

Photocathode	Photocurrent density at 0 V vs. RHE (mA cm^{-2})	Onset potential (V vs. RHE)	HC-STH (%)	Potential at maximum HC-STH (V vs. RHE)	Reference
Pt-containing state-of-the-art photocathodes					
Pt/CdS/CIGS	–28	0.75	12.5	0.53	1
Pt/TiO_2/n^+p-Si	–20.3	0.64	8.1	0.43	2
Pt/Mo/Ti/CdS/$(ZnSe)_{0.85}(CIGS)_{0.15}$	–12	0.89	3.6	0.45	3
Pt/CdS/$(CuInS_2)_{0.81}(ZnS)_{0.19}$	–16.7	0.84	5.6	0.45	4
Pt/TiO_2/CdS/SnS/Au	–19	0.25	0.7	0.08	5
Pt/TiO_x/BHJ/CuO_x	–7.3	0.63	1.5	0.3	6
Pt/TiO_2/CdS/Sb_2Se_3/Au	–30	0.5	3.4	0.26	7
Pt-free state-of-the-art photocathodes					
CuO/$CuBi_2O_4$	–0.9 (at 0.1 V vs. RHE)	1	0.19	0.3	8
Ni-Mo/CdS/CIGS	–25	0.5	2.8	0.24	9
CoP_2/TiO_2/AZO/p-Si	–16.7	0.48	2.22	0.22	10
MoS_x/CdS/CZTS	–18	0.6	3	0.3	11
MoS_2/Ti foil/In-Ga eutectic alloy/$MAPbI_3$ with L-Proline	–20.6	1.02	11.07	0.63	This study

Table S2 Photoelectrochemical (PEC) performance of previously reported state-of-the-art photocathodes using the MoS_2 HER catalyst.

Photocathode	Photocurrent density at 0 V vs. RHE ($mA\ cm^{-2}$)	Onset potential (V vs. RHE)	HC-STH (%)	ABPE (%)	Reference
MoS_2/p-Si	–24.6	0.17	–	0.86	12
$CoMoS_x$/p-Si	–17.2	0.19	–	0.72	13
MoS_2/p-GaN	–2.15	0.8	–	3.18	14
Rh-P/MoS_2/TiO_2/p-Si	–24.1	0.43	–	2.12	15
MoS_x/In_2S_3/Sb_2Se_3	–27	0.89	2.6	2.6	16
MoS_2/TiO_2/n^+p-Si	–33.7	0.46	–	4.9	17
Pt/Ni-MoS_x/$CuInS_2$	–15.5	0.5	1.48	–	18
MoS_x/CdS/CZTS	–18	0.6	3	–	11
MoS_2/Ni_3S_2/Ni/n^+np^+-Si	–41.6	0.54	–	11.2	19
MoS_2/Ti foil/In-Ga eutectic alloy/$MAPbI_3$ with L-Proline	–20.6	1.02	11.07	11.75	This study

References

1 H. Kobayashi, N. Sato, M. Orita, Y. Kuang, H. Kaneko, T. Minegishi, T. Yamada and K. Domen, *Energy Environ. Sci.*, 2018, **11**, 3003–3009.

2 C. Ros, T. Andreu, M. D. Herna´ndez-Alonso, G. PenelasPe´rez, J. Arbiol and J. R. Morante, *ACS Appl. Mater. Interfaces*, 2017, **9**, 17932–17941.

3 H. Kaneko, T. Minegishi, M. Nakabayashi, N. Shibata and K. Domen, *Angew. Chem., Int. Ed.*, 2016, **128**, 15555–15559.

4 J. Zhao, T. Minegishi, H. Kaneko, G. Ma, M. Zhong, M. Nakabayashi, T. Hisatomi, M. Katayama, N. Shibata, T. Yamada and K. Domen, *Chem. Commun.*, 2019, **55**, 470–473.

5 H. Lee, W. Yang, J. Tan, J. Park, S. G. Shim, Y. S. Park, J. W. Yun, K. M. Kim and J. Moon, *ACS Appl. Mater. Interfaces*, 2020, **12**, 15155–15166.

6 W. Shi, W. Yu, D. Li, D. Zhang, W. Fan, J. Shi and C. Li, *Chem. Mater.*, 2019, **31**, 1928–1935.

7 W. Yang, J. H. Kim, O. S. Hutter, L. J. Phillips, J. Tan, J. Park, H. Lee, J. D. Major, J. S. Lee and J. Moon, *Nat. Commun.*, 2020, **11**, 861.

8 S. Pulipaka, N. Boni, G. Ummethala and P. Meduri, *J. Catal.*, 2020, **387**, 17–27.

9 M. Baek, M. Zafar, S. Kim, D. H. Kim, C. W. Jeon, J. Lee and K. Yong, *ChemSusChem*, 2018, **11**, 3679–3688.

10 H. Li, P. Wen, D. S. Itanze, M. W. Kim, S. Adhikari, C. Lu, L. Jiang, Y. Qiu and S. M. Geyer, *Adv. Mater.*, 2019, **31**, 1900813.

11 K. Feng, D. Huang, L. Li, K. Wang, J. Li, T. Harada, S. Ikeda and F. Jiang, *Appl. Catal., B*, 2020, **268**, 118438.

12 K. C. Kwon, S. Choi, K. Hong, C. W. Moon, Y.-S. Shim, D. H. Kim, T. Kim, W. Sohn, J.-M. Jeon, C.-H. Lee, K. T. Nam, S. Han, S. Y. Kim and H. W. Jang, *Energy Environ. Sci.*, 2016, **9**, 2240–2248.

13 C.-J. Chen, K.-C. Yang, C.-W. Liu, Y.-R. Lu, C.-L. Dong, D.-H. Wei, S.-F. Hu and R.-S. Liu, *Nano Energy*, 2017, **32**, 422–432.

14 D. Ghosh, P. Devi and P. Kumar, *ACS Appl. Mater. Interfaces*, 2020, **12**, 13797–13804.

15 Z. Chen , Y. Li , L. Wang , Y. Bu and J.-P. Ao, *J. Mater. Chem. A*, 2021, **9**, 9157–9164.

16 C. Liu, T. Liu, Y. Li, Z. Zhao, D. Zhou, W. Li, Y. Zhao, H. Yang, L. Sun, F. Li and Z. Li, *J. Mater. Chem. A*, 2020, **8**, 23385–23394.

17 W. Xun, Y. Wang, R. Fan, Q. Mu, S. Ju, Y. Peng and M. Shen, *ACS Energy Lett.*, 2021, **6**, 267–276.

18 J. Zhao, T. Minegishi, G. Ma, M. Zhong, T. Hisatomi, M. Katayama, T. Yamada and K. Domen, *Sustainable Energy Fuels*, 2020, **4**, 1607–1611.

19 R. Fan, J. Zhou, W. Xun, S. Cheng, S. Vanka, T. Cai, S. Ju, Z. Mi and M. Shen, *Nano Energy*, 2020, **71**, 104631.